Journal Name

ARTICLE TYPE

Cite this: DOI: 00.0000/xxxxxxxxxx

Ultrafast Transient Absorption Measurements of Photocarrier Dynamics in $PdSe_2$

Guili Li,[a] Xiaoxian Zhang,[a] Yongsheng Wang,[a] Zhiying Bai,[a] Hui Zhao,[b] Jiaqi He*[c] and Dawei He *[a]

Received Date
Accepted Date

DOI: 00.0000/xxxxxxxxxx

We investigate the photocarrier dynamics in bulk $PdSe_2$, a layered transition metal dichalcogenide with a novel pentagonal structure and unique electronic and optical properties. Using femtosecond transient absorption microscopy, we study the behavior of photocarriers in mechanically exfoliated bulk $PdSe_2$ flakes at room temperature. By employing a 400 nm ultrafast laser pulse, electron-hole pairs are generated, and their dynamics are probed using an 800 nm detection pulse. Our findings reveal that the lifetime of photocarriers in bulk $PdSe_2$ is approximately 210 ps. Furthermore, by spatially resolving the differential reflection signal, we determine a photocarrier diffusion coefficient of about 7.3 $cm^2\ s^{-1}$. Based on these results, we estimate a diffusion length of around 400 nm and a photocarrier mobility of approximately 300 $cm^2\ V^{-1}\ s^{-1}$. These results shed light on the ultrafast optoelectronic properties of $PdSe_2$, offer valuable insights into photocarriers in this emerging material, and enable design of high-performance optoelectronic devices based on $PdSe_2$.

1 Introduction

The successful preparation of graphene has sparked significant interest in two-dimensional layered materials with unique optical, electrical, chemical, and thermal properties. In particular, layered transition metal dichalcogenides (TMDCs) have garnered extensive attention from researchers over the past decade due to their excellent charge transport and thermoelectric properties, layer-dependent electronic band structures, and good air stability.[1–3] MoS_2, in particular, with a moderate carrier mobility and a sizable band gap, has been widely studied.[4,5] The successful fabrication of field-effect transistors (FETs) based on monolayer MoS_2 was reported in 2011.[6,7] However, its relatively large band gap (1.2-1.9 eV)[8] and the narrow tunable band gap range hinders its optimal use in optoelectronic devices. Black phosphorus, which has also been extensively studied, offers a widely tunable band gap (0.3-2 eV); however, its air instability poses a significant challenge for practice devices.[9,10] Similarly, the more recently investigated Bi_2O_2Se system exhibits a narrow band gap (approximately 0.8 eV), limiting its application in visible optoelectronics.[11,12]

In contrast to most TMDCs, $PdSe_2$ offer wide tunability of its physical properties by its thickness. For example, it band gap changes from 1.43 eV in a monolayer to 0.6 eV in bulk.[13] With small band gaps, it can be used to manufacture near-infrared photodetectors, sensors, and other devices with high sensitivity and high stability. Additionally, $PdSe_2$ exhibits high carrier mobility,[14] in-plane optical anisotropy,[15] and remarkable air stability.[16] FETs with $PdSe_2$ as the channel material have been demonstrate, with high charge mobilities and superior bipolar characteristics.[17] Theoretical calculations have predicted that the carrier mobility of pentagonal two-dimensional $PdSe_2$ can exceed 1000 cm^2/Vs, while experimentally achieved values are below 300 cm^2/Vs.[13,14,18,19] While such a mobility is moderate compared to other narrow-gap 2D materials, the high stability of $PdSe_2$ in air enhances the operational lifetime of devices in complex environments. Furthermore, $PdSe_2$-based photodetectors demonstrate excellent performance, such as ultra-wideband spectral detection, ultrafast response and high sensitivity.[20–22] For instance, $PdSe_2$ photodetectors have achieved a responsivity of 708 A W^{-1} and a detectivity of 1.31×10^9 Jones.[23]

In additional to these applications as individual material, $PdSe_2$ has also been used to fabricate heterostructures for photodetectors with exceptional performance. A $PdSe_2/MoS_2$ van der Waals heterostructure photodetector demonstrated a detectivity as high as 8.21×10^9 Jones, with excellent photocurrent response time.[20] Likewise, a $PdSe_2/WS_2$ heterostructure device exhibits a broadband spectral light response from 532 to 1550 nm, with a response time of less than 100 ms.[24] However, despite the early study of $PdSe_2$ dating back to 1957,[25] the dynamic properties of

[a] *Key Laboratory of Luminescence and Optical Information, Ministry of Education, Institute of Optoelectronic Technology, Beijing Jiaotong University, Beijing 100044, China. E-mail: dwhe@bjtu.edu.cn*

[b] *Department of Physics and Astronomy, The University of Kansas, Lawrence, Kansas 66045, USA. E-mail: huizhao@ku.edu; Fax: +1 785 864 5262; Tel: +1 785 864 1938*

[c] *College of Mathematics and Physics, Beijing University of Chemical Technology, Beijing 100029, China. E-mail: jqhe@buct.edu.cn*

photocarrier in $PdSe_2$ have not been fully explored. These properties are crucial for the future design and optimization of FET and photodetectors based on $PdSe_2$ and its heterostructures.

In this study, we investigate the dynamics of photocarriers in mechanically exfoliated thick flakes of $PdSe_2$ using time-resolved and spatially-resolved transient absorption microscopy. We determine a lifetime of photocarriers in bulk $PdSe_2$ of approximately 210 ps, a diffusion coefficient is approximately 7.3 $cm^2\ s^{-1}$, and a diffusion length of around 400 nm. The carrier lifetime is a critical factor that significantly impacts the performance of optoelectronic devices. For instance, in solar cells, the photocarrier lifetime determines the power conversion efficiency. The diffusion length of the photocarriers has a significant impact on the performance of semiconductor optoelectronic devices, such as photodiodes and solar cells. In these devices, the diffusion length of the photocarriers determines the distance the photocarriers can reach during their lifetime, and thus impacts the detectivity and efficiency of these devices. The findings presented in this study offer valuable insights into the comprehension, design, development, and optimization of high-performance optoelectronic devices based on $PdSe_2$. Investigations of the ultrafast photocarrier dynamics also provide insights into the underlying physical mechanisms and enable the development of new device architectures and applications with improved performance.

2 Experimental Section

In this study, we utilized high-purity crystals of $PdSe_2$ obtained from 2D Semiconductor. The bulk $PdSe_2$ sample was prepared by mechanically exfoliating flakes from a crystal onto a polydimethylsiloxane (PDMS) substrate using an adhensive tape. Subsequently, a dry transfer technique was employed to transfer the exfoliated $PdSe_2$ flakes onto a SiO_2/Si substrate. During the optical microscopic examination, it was observed that thicker flakes exhibit higher contrasts. Therefore, by comparing the microscopic images, we were able to select the flakes of appropriate thickness for our experiments. We chose samples that exhibited relatively high contrasts so that they can be treated as bulk crystals.

The photocarrier dynamics in $PdSe_2$ is studied by using a home-built transient absorption microscopy setup with space-time resolution capabilities, as illustrated in Fig. 1. An 80-MHz femtosecond titanium sapphire oscillator (MAI TAI HP by Newport) outputs ultrashort pulses with a temporal width of less than 100 fs and a wavelength range of 690-1040 nm. For our experimental requirements, the MAI TAI was adjusted to output 800-nm pulses.

The 800-nm pulse is divided into two parts through a beam splitter. One part is used as the probe pulse for the measurement, while the other part is used to generate a pump pulse of 400 nm, by passing it through a $\beta-$barium borate (BBO) crystal. The pump pulse is directed to the sample for photoexcitation of the carriers. The probe pulse is subsequently delivered to the sample after a delay produced by a motorized translation stage. The two pulses are spatially overlapped. When the optical path lengths of the probe and pump are equal, the two pulses arrive at the sample simultaneously, which is defined as zero delay ($\Delta t = 0$). During the experiment, half-wave plates (HWPs) are used to adjust the power of the pump and probe pulses, and polarizers (PZs) are used to adjust their polarization state. A photodetector is used to detect the power of the probe pulse that is reflected off the sample, converting it to an electrical signal. A lock-in amplifier is utilized to collect and record the signal on a computer. To achieve a higher signal-to-noise ratio with the lock-in amplifier, a chopper is used to modulate the pump pulse. With this configuration, the lock-in amplifier measured the change of the detected probe power induced by the pump. This signal is proportional to the differential reflectance, $\Delta R/R_0 = (R - R_0)/R_0$, where R and R_0 are the probe reflectance with and without the pump pulse, respectively.

Building upon this time-resolved system, the introduction of spatially-resolved pump-probe allowed us to investigate the in-plane transport characteristics of photocarriers. By combining ultrafast time and space resolution, we were able to study the dynamics of bulk $PdSe_2$ carriers on the ultrafast timescale and μm length scales. In such measurements, the differential reflection signal was recorded as a function of the spatial distance between the centers of the probe and pump spots. By carefully adjusting the pitch angle of the reflected probe light through controlled tilting of a beam splitter in the probe optical path, the probe light was deviated from normal, enabling continuous variation of the relative position of the two spots and thus measurement of the differential reflection signal as a function of the probe delay and the probe position. Throughout the measurements, the sample was maintained at room temperature under ambient conditions.

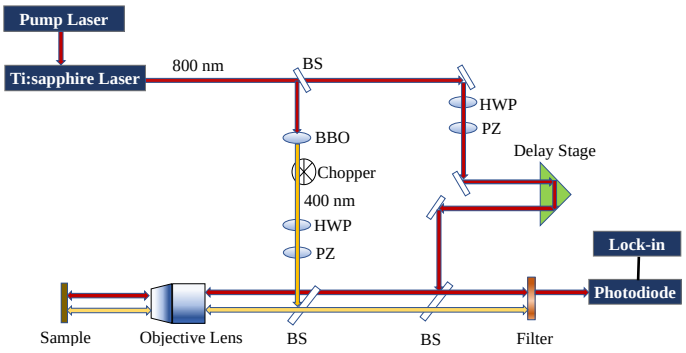

Fig. 1 Schematics of the transient absorption microscopy setup.

3 Results and Discussion

Unlike the 1T, 2H, and 1T' structures commonly found in most 2D TMDCs,[26,27] $PdSe_2$ has a folded pentagonal atomic structure with an orthogonal lattice arrangement,[28] as shown in Fig. 2a. In this structure, each Pd atom forms covalent bonds with four Se atoms, and the Se atoms within a single layer are bonded to each other.[29] The layers are connected through van der Waals forces, making the structure highly stable.

The optical microscope image of the bulk $PdSe_2$ sample in Fig. 2b reveals that the sample has an irregular shape with approximate dimensions of 86 × 200 μm^2. To further characterize the sample, a cross-sectional view by atomic force microscopy (AFM) is shown in Fig. 2c, revealing a thickness of approximately 33 nm in Fig. 2d. From the perspectives of electronic properties,

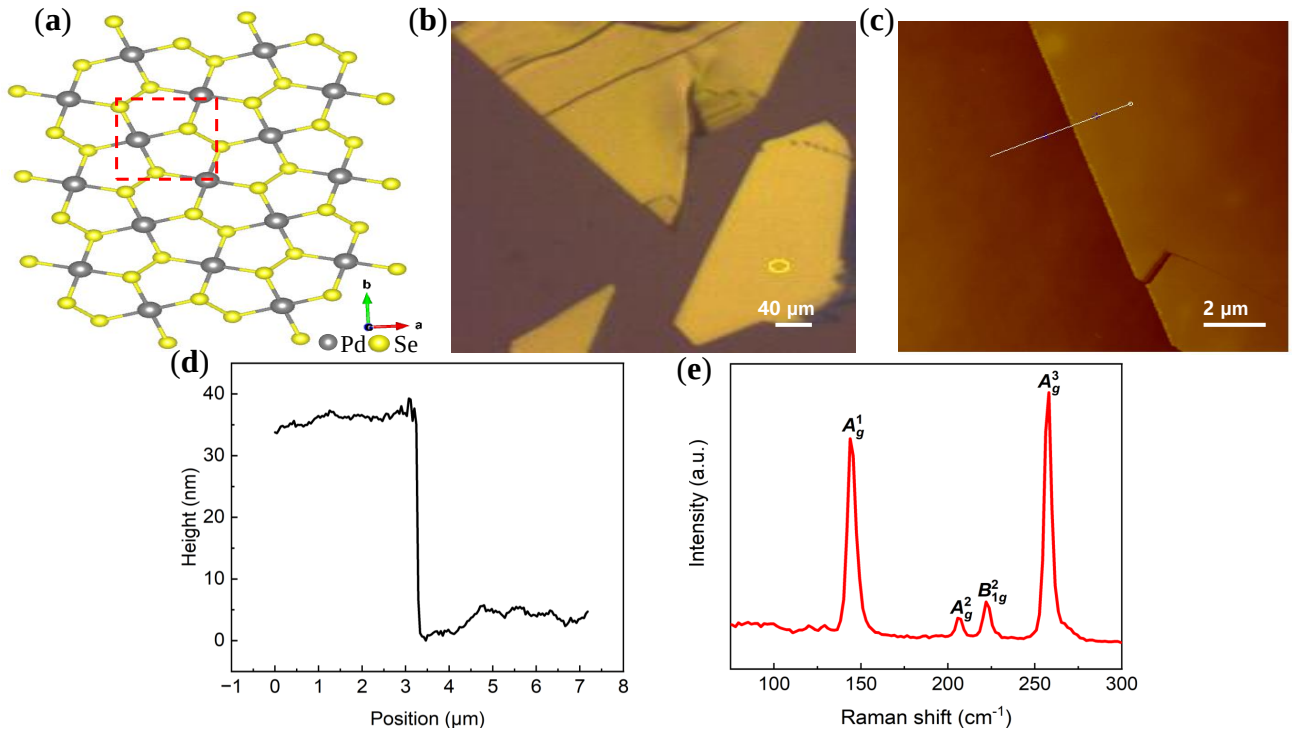

Fig. 2 (a) Crystalline structure of $PdSe_2$. The gray and yellow spheres represent Pd and Se atoms, respectively. (b) Optical microscope image of the bulk $PdSe_2$ sample on a SiO_2/Si substrate. (c) Atomic force microscope image of the $PdSe_2$ sample. (d) Height profile of the sample along the white line shown in panel c, indicating a sample thickness of approximately 33 nm. (e) Raman spectrum of the $PdSe_2$ sample shown in (b) measured with a 532 nm laser beam.

the sample can be viewed as a bulk crystal as its electronic band structure is expected to be bulk-like.

The Raman spectrum of the $PdSe_2$ sample is obtained at room temperature using a 532 nm laser, as depicted in Fig. 2e. The spectrum exhibits four distinct Raman characteristic peaks located at approximately 144 cm^{-1}, 206 cm^{-1}, 222 cm^{-1}, and 257 cm^{-1}. These peaks are in good agreement with those reported in literature for $PdSe_2$.[15,30] The observed peaks are sharp, indicating the high quality of the sample. Specifically, the four peaks correspond to the A_g^1, A_g^2, B_{1g}^2 and A_g^3 vibrational modes, respectively. The A_g^1, A_g^2 and B_{1g}^2 modes primarily arise from the motion of the Se atoms, whereas the A_g^3 mode (located at approximately 257 cm^{-1}) is associated with the relative motion between Pd and Se atoms.

Next, we performed transient absorption measurements using an 800-nm probe and a 400-nm pump to obtain the time-resolved differential reflection signal of the sample at different pump fluences. A combined experimental and computational study shew that bulk-like $PdSe_2$ has an indirect band gap of about 0.6 eV and a direct band gap of about 1.0 eV at its Γ point.[31] Hence, the 400-nm (3.10-eV) pump excites photocarriers with large excess energies. The 800-nm (1.55-eV) probe coupled to the direct transitions in the high energy states in the Γ valley, and thus monitors carrier density in these states. However, since the carrier system form a thermal distribution, these carriers represents the overall carrier population and its dynamics. Fig. 3a and 3b show examples of the observed differential reflection signals in the short (a) and long time ranges (b), respectively. It has been reported that the absorption coefficient of $PdSe_2$ at 400 nm is 5×10^8 m^{-1}.[32] Using this value, the areal carrier density injected by a fluence of 1 μJ cm^{-2} at the center of the pump spot and at the front surface of the sample is approximately 2×10^{12} cm^{-2}.

The time-resolved differential reflection measurement of bulk $PdSe_2$ reflects the evolution of the photocarrier density in the sample following their injection by the pump pulse. As depicted in Fig.3a, the signals at various pump fluences exhibit a rapid rise immediately after excitation. Following the peak, the signal decay can be fitted with a double exponential function:

$$\Delta R/R_0(t) = A_1\exp(-t/\tau_1) + A_2\exp(-t/\tau_2) + B,$$

as illustrated by the curves in Fig. 3a. The two decay time constants deduced are plotted in Fig. 3d. We find that these time constants are independent of the pump fluences. The long time constant of approximately 210 ps represents the lifetime of the photocarriers. Notably, this carrier recombination lifetime is longer than that of commonly studied two-dimensional bulk TMDCs, such as WS_2 (110 ps),[33] $MoTe_2$ (80 ps),[34] and MoS_2 (180 ps).[35]. The short time constant of about 0.87 ps could be attributed to the exciton formation process, as has been generally observed in other TMDCs .[36–38] Fig.3c depicts the relationship between the peak differential reflection signal and the pump fluence. The plot shows that the peak signal is proportional to the pump fluence, further confirming that the differential reflectance is proportional to the carrier density.

To investigate the in-plane transport properties of photocarri-

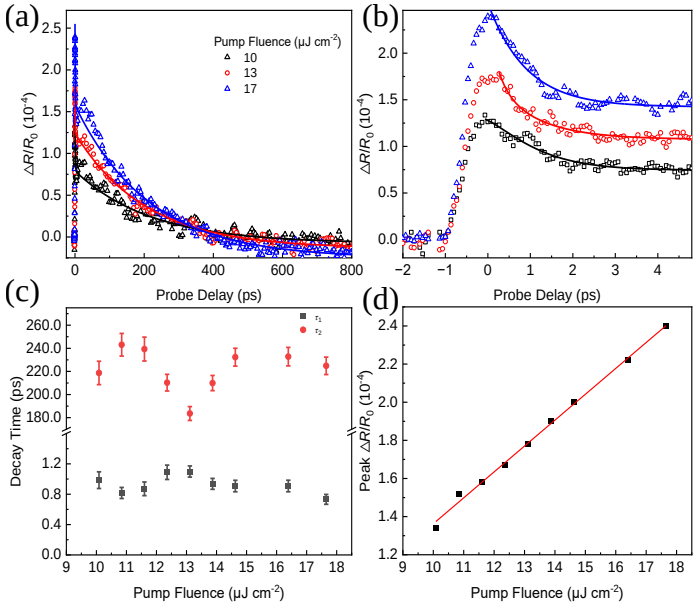

Fig. 3 (a) Differential reflection signal of the bulk $PdSe_2$ sample as a function of the probe delay measured with an 800 nm probe and a 400 nm pump pulses with various fluences. Curves are exponential fits. (b) The same as (a) but with a shorter range of probe delays. (c) The decay time constants deduced from the fits shown in (b) as a function of the pump fluence. (d) Peak differential reflection signal as a function of the pump fluence. The red line is a linear fit.

ers in bulk $PdSe_2$, we conduct a spatially resolved measurement. Fig. 4a illustrates the temporal and spatial evolution of the signal, obtained by scanning the probe delay and position. Driven by the density gradient, the photocarriers are expected to diffuse laterally, resulting in the spatial broadening of the Gaussian distribution over time. Fig.4b presents some examples of the spatial distributions of the differential reflection signal measured at different probe delays of 18 ps (green), 41 ps (yellow), 63 ps (blue), and 81 ps (orange), respectively, along with their Gaussian fits (curves). Fig.4c illustrates the squared Gaussian width as a function of the probe delay. This relation provides insights into the carrier diffusion dynamics and enables the determination of important transport parameters.

Classical diffusion-recombination model reveals that for photocarriers with an initial Gaussian spatial distribution, the spatial profile maintains a Gaussian shape throughout the diffusion and recombination process. The full-width at half-maxima of the spatial profile evolves as

$$w^2(t) = w_0^2 + 16\ln(2)Dt$$

here, D and w_0 denote the carrier diffusion coefficient and the initial Gaussian profile width.[39] The red line in Fig. 4c represents a linear fit, from which we extract a diffusion coefficient of 7.3 $cm^2\ s^{-1}$. Multiple measurements were performed on this sample, and similar results have been obtained as shown in Fig. S1 and Fig. S2, Supporting Information.

Using the lifetime (210 ps) obtained above, the diffusion length (L) in bulk $PdSe_2$ can be calculated as 400 nm. Furthermore, by applying the Einstein relation, a photocarrier mobility of approximately 300 $cm^2\ V^{-1}\ s^{-1}$ can be obtained. This mobility value is comparable to those reported in the literature [14] and highlights the advancements in optoelectronic device fabrication technology. It is worth noting that the diffusion coefficient and diffusion length measured in our experiment are larger than the previously reported values of typical TMDC crystals. For instance, the diffusion coefficient and length bulk WS_2 is 3.5 $cm^2\ s^{-1}$ and 196 nm, respectively,[33] and 4.2 $cm^2\ s^{-1}$ and 270 nm, respectively, in bulk MoS_2.[35]

Other basic parameters of carrier dynamics can be extracted from these results. The observed diffusion of carriers is driven by density gradients through thermal motion of the carriers. At room temperature, the thermal velocity of the carriers is approximately 10^5 m/s. With a diffusion coefficient of 7.3 $cm^2\ s^{-1}$, the corresponding mean free time is 0.073 ps, and the mean free path is 7.3 nm. The insights gained into carrier dynamics and transport properties provide a theoretical basis for the development of new microdevices based on $PdSe_2$ in the fields of optoelectronics and electronics.

4 Conclusions

This study provides insights into the dynamical behavior of photocarriers in bulk $PdSe_2$ using spatiotemporally resolved transient absorption microscopy. We obtain a recombination lifetime of approximately 210 ps, a photocarrier diffusion coefficient of approximately 7.3 $cm^2\ s^{-1}$, a diffusion length of about 400 nm, and a mobility of around 300 $cm^2\ V^{-1}\ s^{-1}$. These findings enhance our understanding of optoelectronic properties of $PdSe_2$. This knowledge serves as a solid foundation for future material advancements and provides a basis for designing optoelectronic devices with optimal performance using this novel material.

Conflicts of interest

The authors declare no conflict of interest.

Acknowledgements

We are grateful for the financial support of the National Natural Science Foundation of China (Grant No. 61975007) and the Beijing Natural Science Foundation (Grant Nos. Z190006 and 4222073). H.Z. acknowledges support by the U.S. Department of Energy (DE-SC0020995).

Notes and references

1 D. Jariwala, A. R. Davoyan, J. Wong and H. A. Atwater, *Acs Photonics*, 2017, **4**, 2962–2970.
2 K. S. Novoselov, A. Mishchenko, o. A. Carvalho and A. Castro Neto, *Science*, 2016, **353**, aac9439.
3 Y. Pan, L. Zhang, L. Huang, L. Li, L. Meng, M. Gao, Q. Huan, X. Lin, Y. Wang, S. Du *et al.*, *small*, 2014, **10**, 2215–2225.
4 B. Radisavljevic, A. Radenovic, J. Brivio, V. Giacometti and A. Kis, *Nature nanotechnology*, 2011, **6**, 147–150.
5 B. Liu, C. You, C. Zhao, G. Shen, Y. Liu, Y. Li, H. Yan and Y. Zhang, *Chinese Optics Letters*, 2019, **17**, 020002.
6 J. N. Coleman, M. Lotya, A. O'Neill, S. D. Bergin, P. J. King,

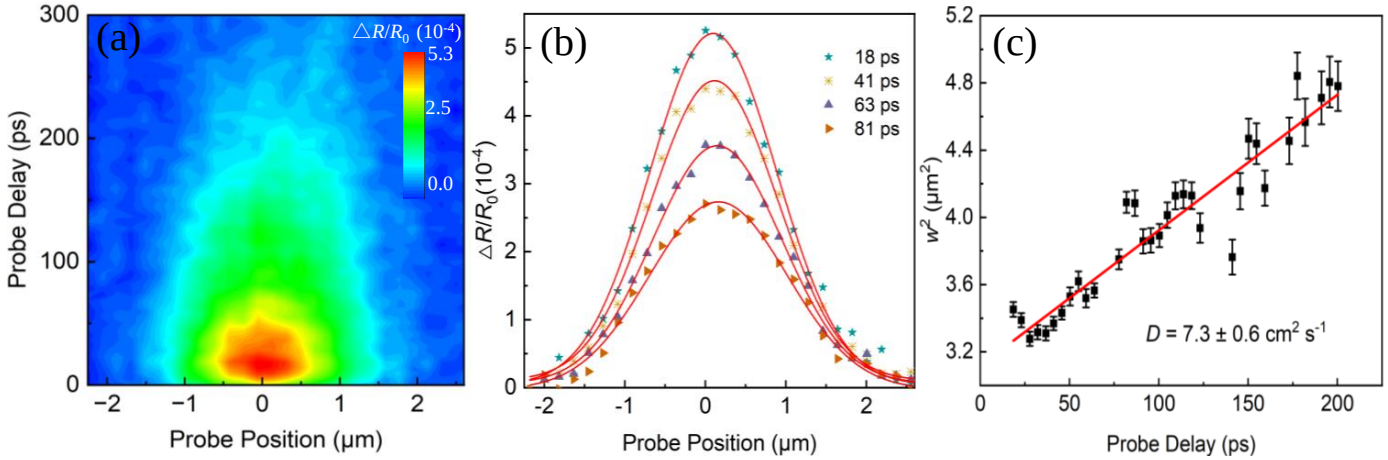

Fig. 4 (a) Differential reflection signal of the bulk $PdSe_2$ sample as a function of both the probe delay and the probe position. (b) Examples of the spatial profiles of the differential reflection signal at probe delays as labeled in the figure. The red curves are Gaussian fits. (c) The squared width of the spatial profiles obtained by Gaussian fits as a function of the probe delay. The linear fit, shown as the red line, gives a diffusion coefficient of about 7.3 $cm^2\ s^{-1}$.

U. Khan, K. Young, A. Gaucher, S. De, R. J. Smith *et al.*, *Science*, 2011, **331**, 568–571.

7 K. F. Mak, C. Lee, J. Hone, J. Shan and T. F. Heinz, *Physical review letters*, 2010, **105**, 136805.

8 S. Manzeli, D. Ovchinnikov, D. Pasquier, O. V. Yazyev and A. Kis, *Nature Reviews Materials*, 2017, **2**, 1–15.

9 Z.-Y. Ong, G. Zhang and Y. W. Zhang, *Journal of Applied Physics*, 2014, **116**, 214505.

10 V. Tran, R. Soklaski, Y. Liang and L. Yang, *Physical Review B*, 2014, **89**, 235319.

11 J. Wu, C. Tan, Z. Tan, Y. Liu, J. Yin, W. Dang, M. Wang and H. Peng, *Nano letters*, 2017, **17**, 3021–3026.

12 J. Wu, H. Yuan, M. Meng, C. Chen, Y. Sun, Z. Chen, W. Dang, C. Tan, Y. Liu, J. Yin *et al.*, *Nature Nanotechnology*, 2017, **12**, 530–534.

13 J. Sun, H. Shi, T. Siegrist and D. J. Singh, *Applied Physics Letters*, 2015, **107**, 153902.

14 Y. Gu, H. Cai, J. Dong, Y. Yu, A. N. Hoffman, C. Liu, A. D. Oyedele, Y.-C. Lin, Z. Ge, A. A. Puretzky *et al.*, *Advanced Materials*, 2020, **32**, 1906238.

15 A. D. Oyedele, S. Yang, L. Liang, A. A. Puretzky, K. Wang, J. Zhang, P. Yu, P. R. Pudasaini, A. W. Ghosh, Z. Liu *et al.*, *Journal of the American Chemical Society*, 2017, **139**, 14090–14097.

16 A. N. Hoffman, Y. Gu, L. Liang, J. D. Fowlkes, K. Xiao and P. D. Rack, *npj 2D Materials and Applications*, 2019, **3**, 50.

17 D. Qin, P. Yan, G. Ding, X. Ge, H. Song and G. Gao, *Scientific reports*, 2018, **8**, 2764.

18 W. L. Chow, P. Yu, F. Liu, J. Hong, X. Wang, Q. Zeng, C.-H. Hsu, C. Zhu, J. Zhou, X. Wang *et al.*, *Advanced Materials*, 2017, **29**, 1602969.

19 F. A. A. M. X. F. Di Bartolomeo, A.Urban, *Nanotechnology*, 2020, **31**, year.

20 M. Long, Y. Wang, P. Wang, X. Zhou, H. Xia, C. Luo, S. Huang, G. Zhang, H. Yan, Z. Fan *et al.*, *ACS nano*, 2019, **13**, 2511–2519.

21 L.-S. Lu, G.-H. Chen, H.-Y. Cheng, C.-P. Chuu, K.-C. Lu, C.-H. Chen, M.-Y. Lu, T.-H. Chuang, D.-H. Wei, W.-C. Chueh *et al.*, *ACS nano*, 2020, **14**, 4963–4972.

22 J. Zhong, J. Yu, L. Cao, C. Zeng and Y. Liu, *Nano Research*, 2020, **13**, 7.

23 Q. Liang, Q. Wang, Q. Zhang, J. Wei, S. Lim, R. Zhu, J. Hu, W. Wei, C. Lee and C. Sow, *Advanced materials (Deerfield Beach, Fla.)*, 2019, **31**, e1807609.

24 X. Kang, C. Lan, F. Li, W. Wang, S. Yip, Y. Meng, F. Wang, Z. Lai, C. Liu and J. C. Ho, *Advanced Optical Materials*, 2021, **9**, 2001991.

25 F. Grønvold and E. Røst, *Acta Crystallographica*, 1957, **10**, 329–331.

26 M. Chhowalla, H. S. Shin, G. Eda, L.-J. Li, K. P. Loh and H. Zhang, *Nature chemistry*, 2013, **5**, 263–275.

27 A. V. Kolobov and J. Tominaga, *Two-dimensional transition-metal dichalcogenides*, Springer, 2016, vol. 239.

28 C. Soulard, X. Rocquefelte, P.-E. Petit, M. Evain, S. Jobic, J.-P. Itié, P. Munsch, H.-J. Koo and M.-H. Whangbo, *Inorganic chemistry*, 2004, **43**, 1943–1949.

29 M. Jakhar, J. Singh, A. Kumar and K. Tankeshwar, *Nanotechnology*, 2020, **31**, 145710.

30 C.-F. Huo, R. Wen, X.-Q. Yan, D.-K. Li, K.-X. Huang, Y. Zhu, Q. Cui, C. Xu, Z.-B. Liu and J.-G. Tian, *Physical Chemistry Chemical Physics*, 2021, **23**, 20666–20674.

31 M. Wei, J. Lian, Y. Zhang, C. Wang, Y. Wang and Z. Xu, *npj 2D Materials and Applications*, 2022, **6**, 1.

32 C. Ye, Z. Yang, J. Dong, Y. Huang, M. Song, B. Sa, J. Zheng and H. Zhan, *Small*, 2021, **17**, 2103938.

33 J. He, D. He, Y. Wang, Q. Cui, F. Ceballos and H. Zhao, *Nanoscale*, 2015, **7**, 9526–9531.

34 S. Pan, W. Kong, J. Liu, X. Ge, P. Zereshki, S. Hao, D. He, Y. Wang and H. Zhao, *ACS Applied Nano Materials*, 2018, **2**, 459–464.

35 N. Kumar, J. He, D. He, Y. Wang and H. Zhao, *Journal of Applied Physics*, 2013, **113**, 133702.
36 F. Ceballos, Q. Cui, M. Z. Bellus and H. Zhao, *Nanoscale*, 2016, **8**, 11681–11688.
37 P. Steinleitner, P. Merkl, P. Nagler, J. Mornhinweg, C. Schüller, T. Korn, A. Chernikov and R. Huber, *Nano Lett.*, 2017.
38 S. Zhao, D. He, J. He, X. Zhang, L. Yi, Y. Wang and H. Zhao, *Nanoscale*, 2018, 10.1039.C8NR03135E.
39 Ceballos, Frank, Zhao and Hui., *Advanced Functional Materials*, 2017.